JOURNAL OF MATERIALS SCIENCE 31 (1996) 6035–6042

Nanosecond and picosecond laser-induced cracking and ignition of single crystals of ammonium perchlorate

A. L. RAMASWAMY, H. SHIN, R. W. ARMSTRONG, C. H. LEE
University of Maryland, College Park, MD 20742, USA

J. SHARMA
Naval Surface Warfare Center, Silver Spring, MD 20903, USA

Nanosecond and picosecond laser irradiations have been used to study the decomposition of ammonium perchlorate (NH_4ClO_4) crystals, a main component of propellants. Chlorate (NH_4ClO_3) decomposition product was detected via X-ray photoelectron spectroscopy. The decomposition is initiated amid associated mechanical deformations and microcracking processes occurring on a time scale commensurate with actual frequencies of energetic crystal decompositions pertinent to propellant combustion. Optical, scanning electron and atomic force microscopy methods have been applied to characterization of the laser-damage zones. Individual initiation or residual "hot spot" sites have been detected in the electron and atomic force microscope images, and are related to the cracking behaviour of the perchlorate allotropic phases. Evidence of the 240 °C orthorhombic to rock-salt type cubic transformation was obtained in nanosecond laser irradiations through a remnant microstructure of ultrafine cracks whose intersection points marked an array of decomposition sites. A dislocation model description is given for the connected cracking and decomposition site observations.

1. Introduction

Crystals of ammonium perchlorate (AP) constitute one of the most common oxidizers used in propellant mixtures. A solid propellant contains both oxidizer and fuel ingredients that can burn in the absence of air or other oxidizers. The propellant is formulated to burn uniformly and quickly, but without detonating.

Currently, propellants are being used to produce propulsive thrusts in a broad range of applications that include rocket, gun and air-breathing propulsion systems, high-pressure air-bags, high-temperature gases for joining heavy duty electrical cables and other propulsion systems [1]. The substantial applications have made increasingly important the safety issue of developing insensitive propellants. An insensitive composition is one in which there is minimized possibility of initiation as a result of unintentional impact, electrostatic discharge, or thermal and shock stimuli. Detailed understanding of the initiation, ignition and related mechanical deformations of AP crystals is thus of vital importance.

The basic structural mechanisms for the initiation of exothermic reactions in the surface or near-surface layer of energetic materials such as AP are still unclear. Here, the nanosecond and picosecond laser irradiations of such crystals have been used locally to induce the initiation of chemical decomposition amid associated mechanical deformations and microcracking processes all occurring on a time scale commensurate with the actual frequencies of energetic crystal decompositions during propellant burning [2, 3]. Decomposition was detected by X-ray photoelectron spectroscopy (XPS) measurements while the concurrent mechanical deformation and cracking processes associated with the initiation have been revealed via optical, scanning electron and atomic force microscope observations. With the higher resolution of the two latter techniques, residual initiation or "hot spot" sites have been detected and their relation determined to a microscale network of surface cracks. The depths of the surface cracks were measured with a profilometer.

The laser-induced microcracking of the crystals appeared to be intimately involved in the crystal decomposition mechanism(s). The directions of the crack systems have been identified based on the crystallography of two allotropic forms of AP. Upon nanosecond laser irradiation, the crystal exhibited cracking both in the low-temperature orthorhombic structure and after having transformed at higher temperature to a rock-salt cubic structure. The phase transformation had occurred, presumably, at 240 °C. The picosecond laser damage exhibited clear evidence of cracking solely for the orthorhombic structure. The very fine network of cracking in the rock-salt structure relates to propellant burning in a direct way because of the

0022–2461

consideration that a finer network of cracking produces a far greater surface area for the decomposition reaction. The observation that decomposition sites occur at microcrack intersections gives an added importance to obtaining an understanding of how cracking is involved in decomposition mechanisms in energetic crystals. As will be seen, the cracking behaviour is proposed to be an outcome of dislocation movements forced by thermal heating and the consequent orthorhombic to rock-salt-type phase transformation.

2. Experimental procedure

2.1. AP crystals (NH_4ClO_4)

The physical and chemical properties of AP, especially including its thermal stability, have been extensively studied because of the formulation of AP in propellant mixtures [4]. AP decomposes over a wide range of temperatures, extending from 200–530 °C. Single crystals are transparent with an orthorhombic crystal structure containing four molecules per unit cell with $a = 0.9202$, $b = 0.5186$ and $c = 0.7449$ nm. An allotropic phase transformation to the cubic, rock-salt crystal structure occurs at 240 °C, also with four molecules per unit cell and $a = 0.763$ nm. The densities of the orthorhombic and interpenetrating face centred cubic crystal structures are 1.95 and 1.76 g cm^{-3}, respectively [4]. The lower density of the high-temperature polymorph is an important aspect of the compressive cracking behaviour modelled in this study.

Fig. 1 shows an (0 0 1) surface view of a typical crystal of AP used for the laser irradiation experiments. The enclosed ellipsoidal shape is apparently of a "seed" crystal. Fig. 2 is an (0 0 1) stereographic projection representation of the crystal [5]. The crystal is oriented in the lower left inset corner. The principal faces and directions have been identified and labelled. A confirming Laue back-reflection X-ray pattern is superimposed on the stereographic projection. An analysis of zone directions for the Laue "spots" was employed to identify prominent crystal directions as prescribed previously for the orientations of orthorhombic cyclotrimethylenetrinitramine (RDX) crystals [6].

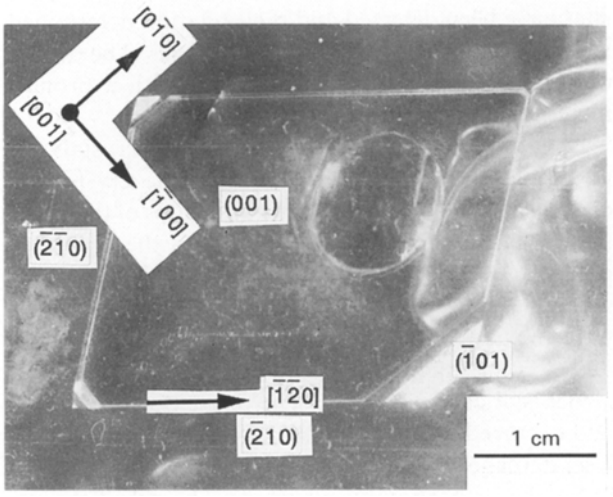

Figure 1 Single crystal of ammonium perchlorate with identified crystal planes and directions.

The absorption spectrum of AP was measured with a standard Fourier transform–infrared spectrometer. The spectrum is shown in Fig. 3. The spectrum only shows the percentage variation in transmittance with wavelength. Absolute values of percentage transmission of the crystal at 1064 nm have to be measured directly. Absorption at the laser wavelength of 1064 nm, corresponding to a wave number of 9398 cm^{-1}, is minimal. A direct measurement of crystal transmittance at 1064 nm gave 0.63 and reflectance, 0.037. From these measurements, an absorptivity, α, in the intensity relationship $I = I_0 \exp(-2\alpha d)$ where d is the thickness of the crystal, gave $\alpha = 2.1 \times 10^{-2}$ mm^{-1}. A correction factor was included for the reflected radiation.

AP is a hygroscopic material, easily absorbing moisture on its surface. The crystals were thus stored in a desiccator and care was taken in all experiments to minimize surface absorption of moisture.

2.2. Laser irradiation

The nanosecond and picosecond laser pulses were obtained from separate Nd/Yag lasers (each 1064 nm in wavelength). The nanosecond laser pulses had a duration of 8 ns (full-width at half maximum, fwhm) and an energy per pulse of 0.25 J. The picosecond laser pulses were 20.6 ps (fwhm) in duration with an energy per pulse of 5.0 mJ. The physical parameters of the two lasers are summarized in Tables I and II. Fig. 4 shows the temporal shape of the nanosecond laser pulse. The spatial profiles of both the nanosecond and picosecond laser pulses are given in Fig. 5a and b, respectively. The nanosecond laser pulse is shown to be inhomogeneous.

The specimen crystals were mounted on to optical microscope slides with the crystal edges fixed by adhesive tape. The beam was focused on to the surface of the crystal so as to give spot sizes of about 1.68 mm for the nanosecond laser pulse and 0.168 mm for the picosecond laser pulse. A schematic illustration of the apparatus for laser irradiation is shown in Fig. 6. The power of the nanosecond laser beam was about 31 MW and the power density was 14 MW mm^{-2}. Similarly, the power for the picosecond laser was about 0.2 GW and the power density was 9 GW mm^{-2}. Positioning of spots on the crystal samples relative to the laser beam was obtained by locating the beam with an infrared sensitive fluorescent strip and then placing the crystal surface directly under the detecting strip.

Laser energy measurements were taken with an Rj-7000 series microprocessor based pyroelectric/silicon energy meter manufactured by Laser Precision Corp. The radiation is collected by an energy probe that is connected to the meter. The latter can average the energy measurements over 100 pulses. When such measurements were taken, the pulse repetition rate of the laser was kept at 1 pulse/second.

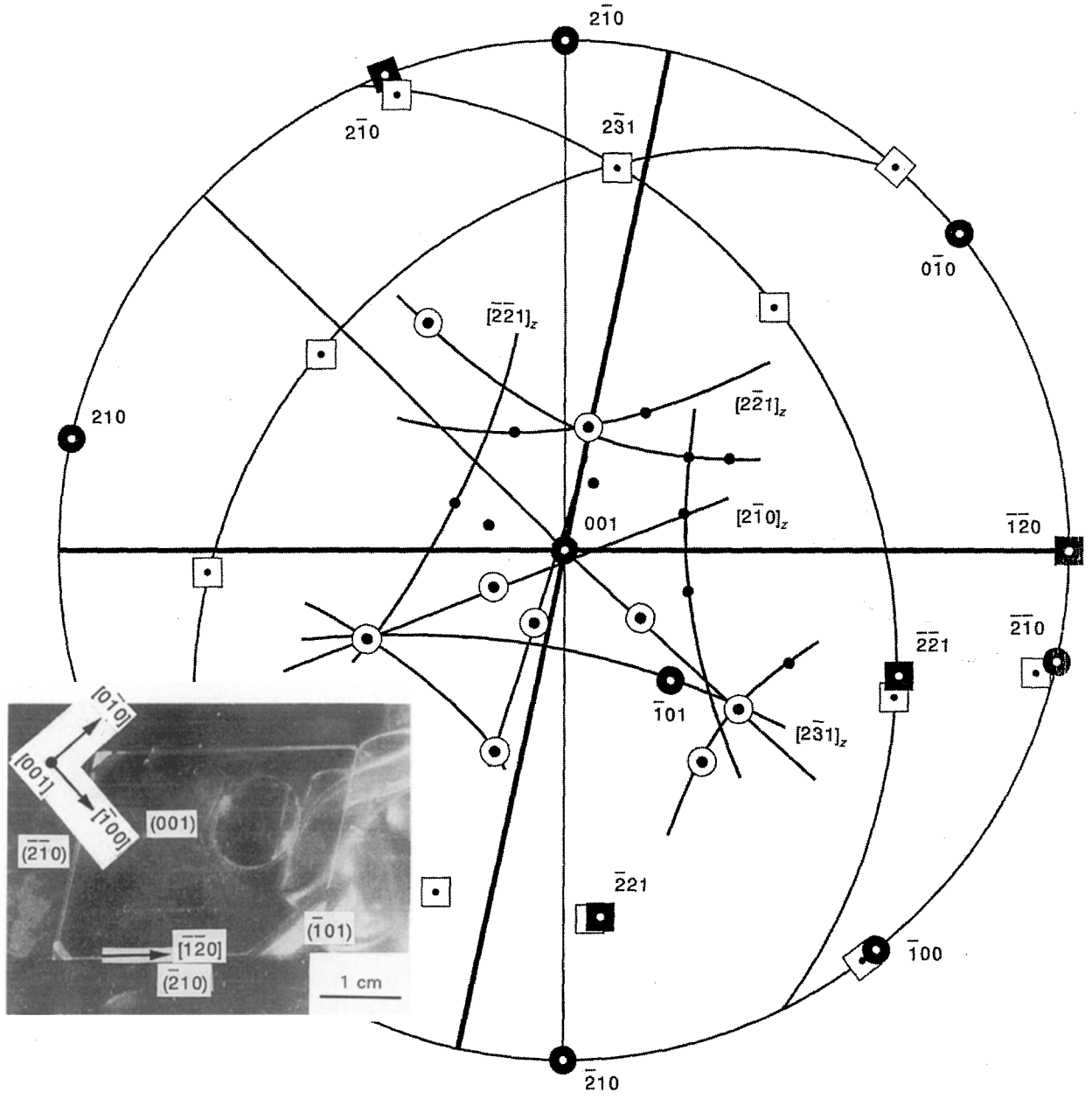

Figure 2 Stereographic projection representation of an AP (0 0 1) crystal surface. A Laue back-reflection X-ray pattern is shown superimposed on the stereographic projection.

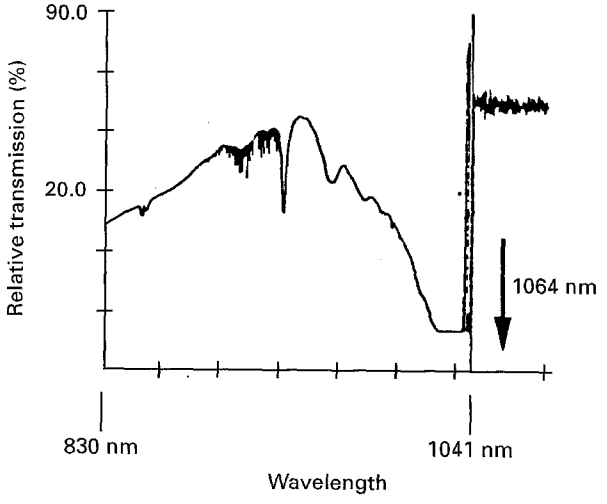

Figure 3 Absorption spectrum for ammonium perchlorate (AP).

TABLE I Nd/Yag nanosecond-pulse laser

Wavelength	1064 nm
Pulse duration (fwhm)	8 ns
Energy without amplifier	13–34 mJ
Energy with amplifier	160–250 mJ
Power	1.6–31 MW
Beam radius	8 mm
Spectral line-width	$< 1\ cm^{-1}$
Power density	> 0.03–$0.62\ MW\,mm^{-2}$

TABLE II Nd/Yag picosecond-pulse laser

Wavelength	1064 nm
Pulse duration (Gaussian)	20.6 ps
Energy	μJ/pulse
Amplified energy	1–5 mJ/pulse
Power	~ 0.2 GW
Beam diameter (Gaussian)	0.8 mm
Power density	$0.4\ GW\,mm^{-2}$

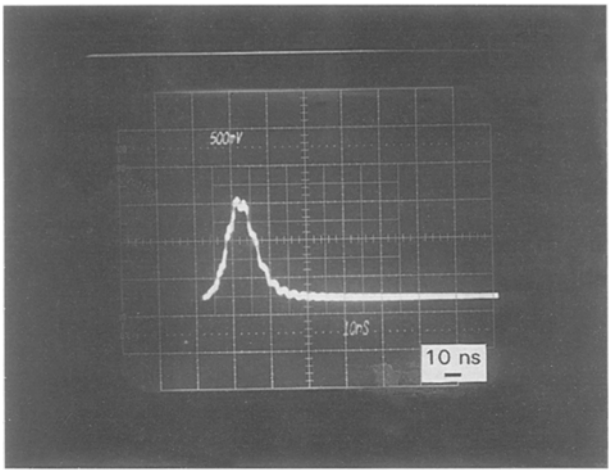

Figure 4 Temporal profile of nanosecond laser pulse.

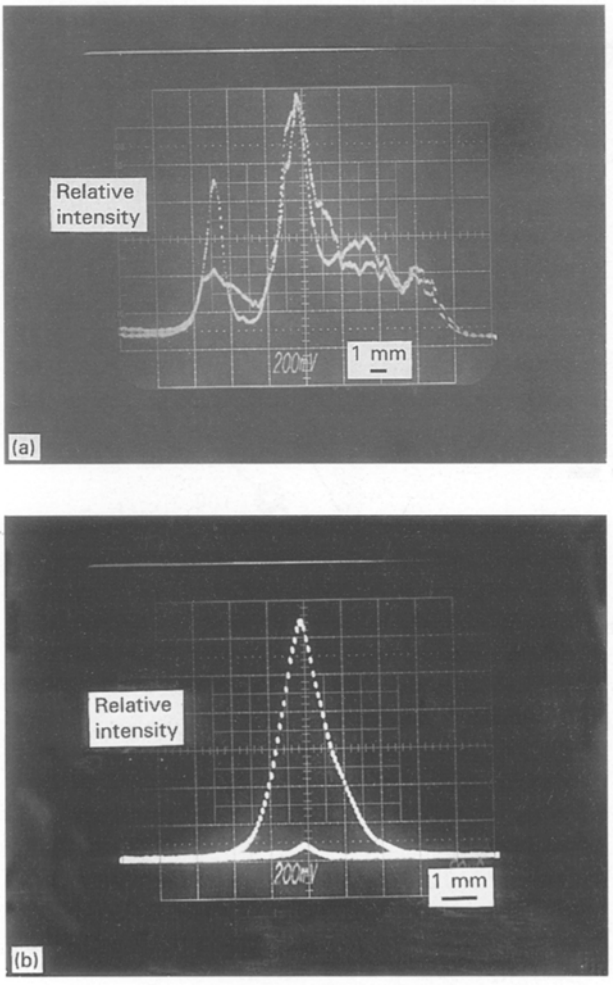

Figure 5 Spatial beam profiles of (a) a nanosecond-laser pulse, (b) a picosecond-laser pulse.

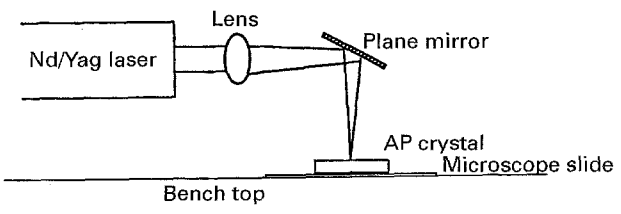

Figure 6 Experimental apparatus for the laser irradiation experiment.

2.3. Microscopy and spectroscopy methods

The surface structures of the irradiated crystals were examined optically in transmission and reflection. An environmental scanning electron microscope (SEM) was also used. An advantage of the environmental SEM is that the samples do not have to be coated with a conductive layer and, also, an inert gas atmosphere can be employed that is convenient for a hygroscopic material such as AP.

A PHI 5400 X-ray photoelectron spectrometer (XPS), with characteristic X-ray lines from a magnesium source (1253.6 eV), was employed for detecting decomposition products [7]. The XPS system was run at −150 kV. The spectrum was run at −15 kV. Unmonochromatized X-rays were used. Every attempt was made to keep the X-ray exposure to a minimum of about 8 min (achieved in time steps), because decomposition caused by the X-rays themselves could add to the previous products from the laser damage. The sampling depth was 5 nm. In this regard, some damage, including cracking, was noted from the X-ray irradiation employed in determining crystal orientations.

Local peak positions and profiles give information about the chemical state of the atom or molecule. The Cl in the ClO_4^- ion has a large binding energy and it shifts to lower values with decrease of oxidation state when new molecular products, such as chlorates and hypochlorites, are formed. The chemical shift is as much as 9 eV between perchlorate and chlorite. The XPS technique has been used here to provide specific information about the progressive decrease in the oxidation state of the chlorine atoms in AP.

A Digital Microprobe II (ver. 5) atomic force microscope (AFM) was used also to examine the very top surface layer structure of the irradiated crystals [8]. For this purpose, the crystal was cleaved to obtain individual slices of about 1 mm thickness and $2 \times 2\,mm^2$ in surface area, that could be mounted under the AFM.

Crack depths were measured on the microscopic scale with an Alpha-Step Profilometer, Model Number 200. The tip of the profilometer is a diamond stylus giving a maximum resolution of 0.5 nm in the vertical direction and a resolution of 40 nm in the horizontal direction. The stylus tip was 1 μm in diameter.

3. Results and discussion

3.1. Laser irradiation

Firstly, the laser damage sites, that could be visually recognized, were examined in reflection and transmission with optical microscopy. Fig. 7 shows, at a normal magnification of ~x150, a reflection micrograph of a nanosecond laser-damage site. A striped array of (0 1 0) cracks was identified for the orthorhombic structure. The same parallel network of cracks was seen in transmission, also. However, closer examination of the crack pattern in reflection showed, in addition, the presence of a finer scale network of cracks that are revealed at higher magnification in Fig. 8. The finer network of orthogonal microcracks is rotated

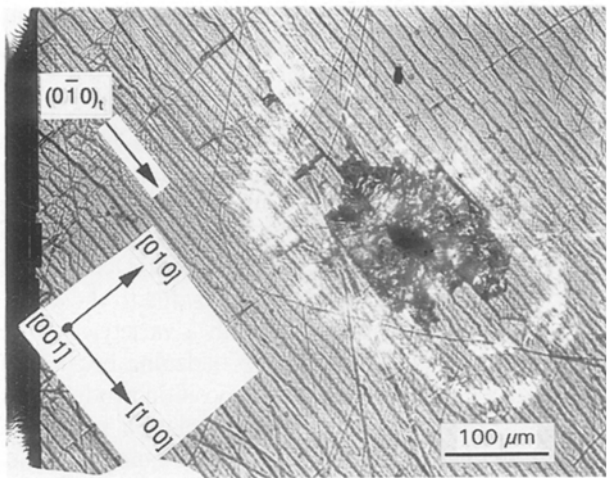

Figure 7 Optical micrograph of nanosecond laser-damage site.

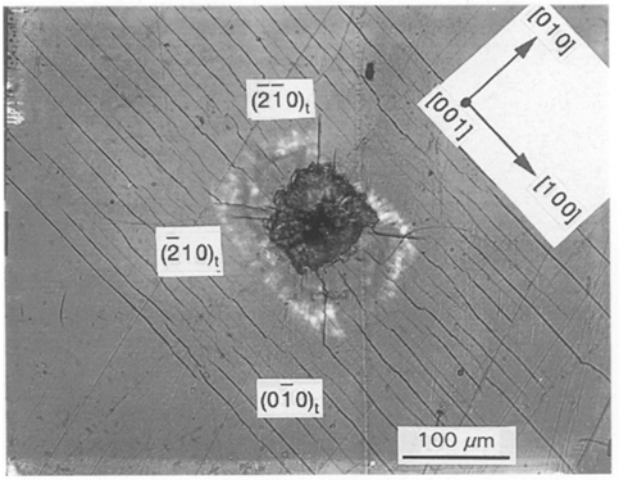

Figure 9 Optical micrograph of a picosecond laser-damage site.

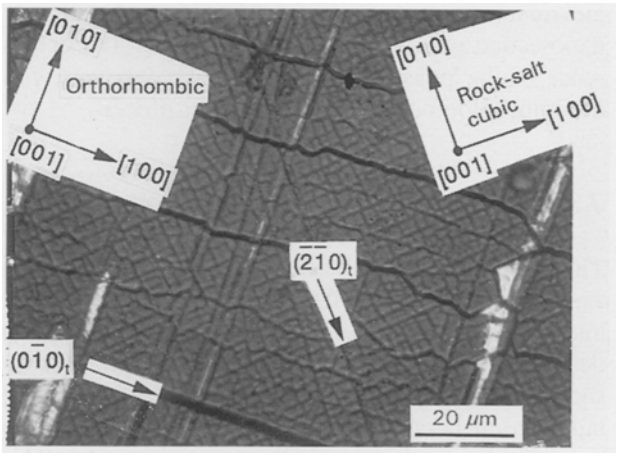

Figure 8 Optical micrograph of nanosecond laser-damage site showing both the cracking due to the orthorhombic and cubic rock-salt crystal structures of AP.

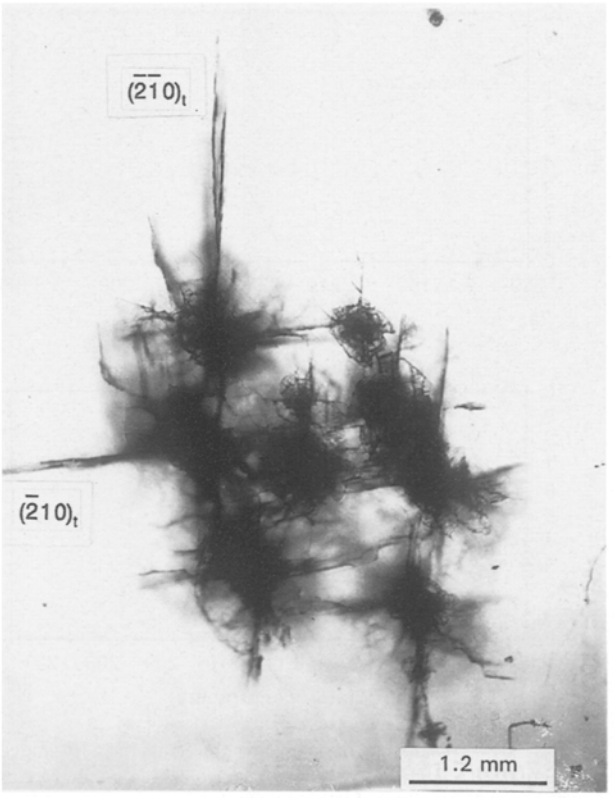

Figure 10 Optical micrograph of a laser-damage site produced by irradiating with 1000 pulses of picosecond duration.

asymmetrically relative to the larger scale (0 1 0) cracks easily recognized in Fig. 7. Calibrated focusing of the optical microscope indicated that the finer cracks were a fraction of a micrometre below the surface of the crystal. The finer scale network does not fit any crack system previously identified [5] for orthorhombic AP and led to the discovery of the crack planes being oriented newly on orthogonal cubic $\{0\,1\,0\}$ based on the known transformation of AP at higher temperature to a rock-salt crystal structure. The transformation is known to occur at 240 °C. The orientation relationship determined for the results in Fig. 8 is $(0\,0\,1)_R \| (0\,0\,1)_O$ with $[1\,0\,0]_R \| [1\,2\,0]_O$ for rock-salt (R) and orthorhombic (O) designations.

Fig. 9 is a reflection micrograph of an analogous laser-damage site produced on the same crystal surface with a picosecond laser pulse. In this case, cracking along the normal orthorhombic $(0\,1\,0)_t$ planes, with t indicating trace, was observed with prominent individual cracks, also, on $(\bar{2}\,\bar{1}\,0)_t$ and $(\bar{2}\,1\,0)_t$ planes of the orthorhombic structure. No evidence of the finer scale microcracking of the rock-salt type cubic structure was observed. The main damage site here is more localized as compared with the nanosecond laser irradiation. This applies as well for sub-surface lateral cracking that is revealed by the encompassing whitish halos in the micrographs of Figs 7 and 9. Fig. 10 shows a transmission micrograph of another laser-damage site produced by irradiating a crystal region with 1000 multiple picosecond laser pulses. Fig. 11 is a reflection micrograph of the same region as in Fig. 10.

The difference in observed microcracking behaviour of the crystal when irradiated with pulses of different duration is an interesting phenomenon. For the picosecond laser pulse, evidence of $\{0\,1\,0\}$ cracking due to the cubic transformation was not detected. A possibility is that the picosecond laser irradiation produced heating and vaporization of material within a more shallow surface layer. In this regard, Figs 7 and

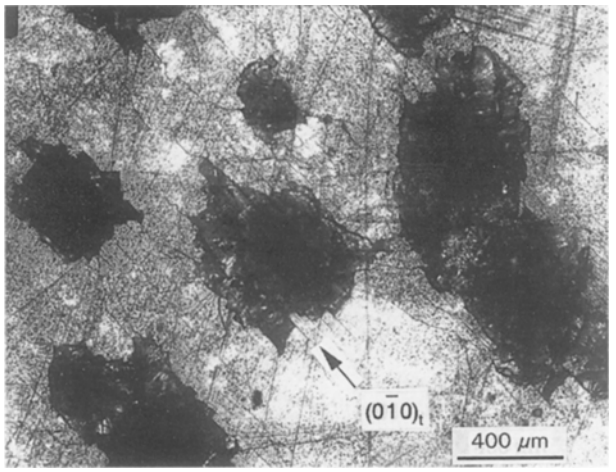

Figure 11 Higher magnification micrograph of the site shown in Fig. 10.

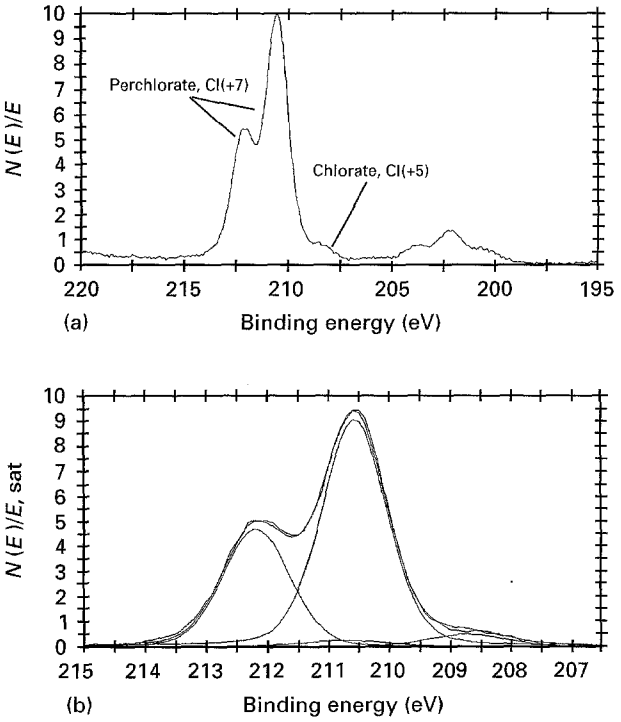

Figure 12 (a) Typical X-ray photoelectron spectrum of an irradiated AP sample. (b) Typical curve-fitting result to estimate the percentage decomposition of the AP sample.

8 show that the residual {0 1 0} cubic cracking structure was not easily visible even for the nanosecond irradiation experiment.

3.2. X-ray photoelectron spectroscopy

The XPS system was applied to the damage sites to detect whether initiation of chemical decomposition had occurred. Fig. 12a shows a typical spectrum in the region of the Cl, 2p level for the irradiated sample. The doublet arises from $2p_{3/2}$ and $2p_{1/2}$ lines of chlorine. A small shoulder on the right-hand side of the $2p_{3/2}$ line at a separation of about 1.7 eV is observable and is indicative of a small amount of decomposition. Curve fitting of the spectra was employed to obtain estimates of the amount of decomposition for the single nanosecond pulse and the 1000 pulses of picosecond irradiation. Fig. 12b gives a typical curve-fitting result. From such curves the decomposition produced by the nanosecond laser irradiation was estimated as ~3% and that produced by the picosecond laser irradiation as ~5%. The decomposition product is ammonium chlorate, NH_4ClO_3. This product is mostly seen in thermal decomposition studies as compared with mechanically impacted samples that show generally the formation of ammonium hypochlorite, NH_4ClO_2, and other lower oxy-acids [4]. The peaks due to the chlorate are very sharp in contrast with a variety of other typical spectra of AP showing broadening because of the presence of a variety of decomposition products. As indicated, the picosecond laser irradiation peak was almost double the size obtained for nanosecond irradiation. The greater decomposition in the case of the picosecond laser pulse can be understood from the fact that the surface had been irradiated with 1000 pulses at individual energy values of 5 mJ compared with one nanosecond pulse at an energy of 250 mJ. The occurrence of the phase transformation is consistent with decomposition occurring in a thermal process.

3.3. Scanning electron microscopy and atomic force microscopy

The surface layer of the laser irradiated crystal was examined in further detail with the environmental SEM and with the atomic force microscope in an effort to detect residual "hot spot" sites of initiation. Fig. 13 shows a scanning electron micrograph of the nanosecond laser damage site. The dark, sub-surface spots are believed to be (hollow) initiation sites. This was confirmed with results obtained with the atomic force microscope, first at low magnification where image details could be matched with the scanning electron micrograph and, then, at higher resolution where the size of decomposition "spots" could be resolved at about 50 nm diameter within a central circular pore structure of the order of 500 nm diameter as in Fig. 14.

The current results are in line with previous investigations where the formation and growth of decomposition nuclei in AP were studied with a microcinematographic apparatus [9]. It was found that the nucleation sites were initiated beneath the surface of crystals. The decomposition centres consisted of spherical nuclei measuring 1–2 μm. Using SEM methods, such decomposition centres, though reported at larger micrometre dimensions as compared with observations

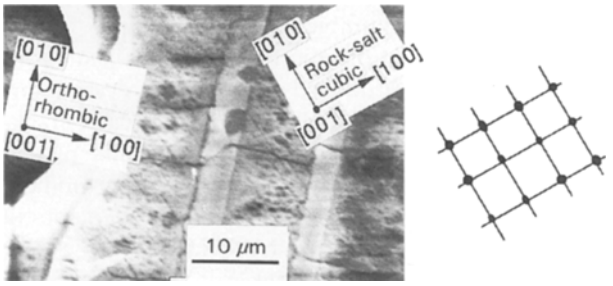

Figure 13 Electron micrograph of nanosecond laser-damage site with a sketch showing the apparent relation between the dark spots or initiation sites and the cubic microcracking.

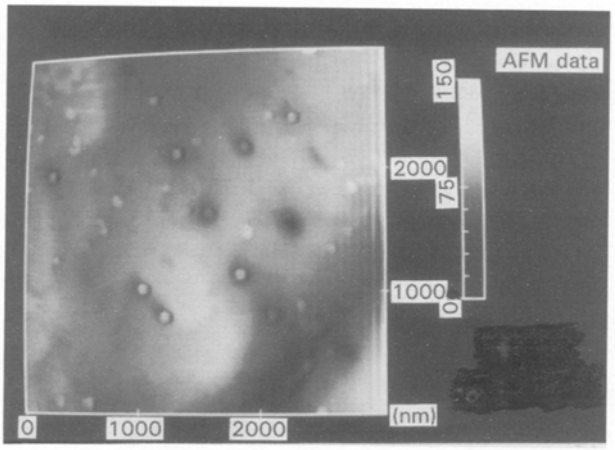

Nanoscope II
Parameters:

Z	100.0 A/V
XY	328.4 A/V
Samples	400/scan

Date taken Wed Oct 05 13:29:16 1994
Buffer 5(LASAP.09), Rotated 0°, XY axis (nm), Z (nm)

Figure 14 Atomic force micrograph of a nanosecond laser-damage site.

reported here, were identified as holes below the crystal surface [10–12]. Current work in the present investigation is centred on the AFM technique in an effort to make further observations at the nanometre scale [13]. The experimental investigations still in progress are to obtain an even deeper understanding of the phenomena.

3.4. Dislocation model

The observed cracking behaviour for both the orthorhombic and cubic structures is important to initiation for one reason because of the increased surface area produced for propellant combustion. Perhaps more importantly, the microcracking provides a clue about mechanical deformation mechanisms occurring in the surface layer of the crystal as a result of the thermomechanical stress state accompanying the laser heating. Profilometer results for the depths of the {0 1 0} microcracks are given in Table III.

Cleavage-type cracks are known to form on {0 1 0} in rock-salt crystals at the intersection of {1 1 0} ⟨1 1 0⟩ slip systems through a dislocation reaction of type [14]

$$(a/2)[0\,1\,\bar{1}]_{(0\,1\,1)} + (a/2)\,[0\,1\,1]_{(0\,\bar{1}\,1)} \rightarrow a[0\,1\,0]_{(0\,0\,1)} \quad (1)$$

Fig. 15 gives a schematic view of the dislocation slip geometry that is predicted to operate for the compressive stress state accompanying thermal heating of the crystal surface layer and, also, transformation to the less dense cubic structure. The reacted $a[0\,1\,0]$ Burgers vector dislocation, with line vector along $[\bar{1}\,0\,0]$, is in the less favourable (0 0 1) slip plane and, further, experiences no movement force. Increased slip of the primary reactant dislocations is proposed to nucleate a multiple

TABLE III Results of profilometer experiments

Area of crystal surface scanned by profilometer tip	Measured crack depths
Smooth undamaged crystal surface	Fluctuations of the profilometer tip detected of the order of 10–42.5 nm
Major cracks or fractures on the surface	Average fracture depth 22.8 μm
Finer surface microcracks	Average depth of fine cracks was 2.3 μm. Finest cracks were 790 nm in depth

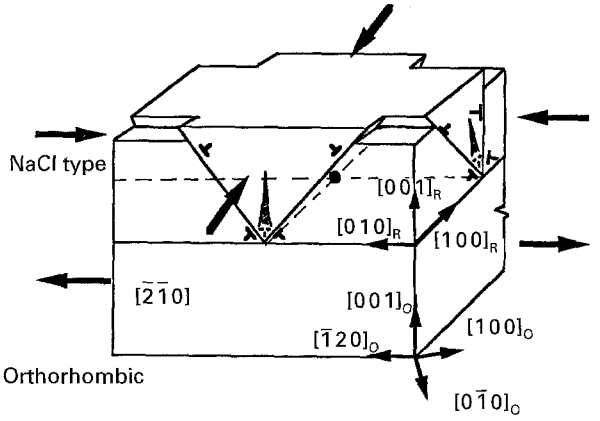

Figure 15 Schematic view of dislocation slip geometry. R, rock-salt; O, orthorhombic.

Burgers vector reacted dislocation at the orthorhombic/cubic structure interface serving as a sub-surface crack nucleus. At sufficient shear stress, the crack nucleus should run vertically upwards to the crystal surface despite the lateral compressive stress state. A similar reaction of slip systems shown on the side (0 1 0) surface of Fig. 15 should give a [1 0 0] crack nucleus on the same basis. The biaxial tensile stress just above the reacted dislocations should add at their points of intersection to give locally a substantial hydrostatic tensile stress state. The situation is fully conducive to generating the hollow decomposition sites observed internally with the SEM and, when sliced through the crystal, with the atomic force microscope. The proposed mechanism is akin to that proposed previously [3] for laser-induced cracking and melting of RDX crystals.

4. Conclusion

Nanosecond and picosecond laser pulses have been used to induce cracking and initiation of chemical decomposition in AP crystals as confirmed with XPS measurements. The detected chlorate decomposition product is the expected result for thermal decomposition; however, there is a thermomechanical aspect to the decomposition results obtained here. Cracking planes consistent with previous studies on orthorhombic AP have been identified and, at a finer scale, residual cracking evidence has been obtained for the transformed cubic structure of AP. A dislocation mechanism is proposed for the cubic microcracking behaviour that is in line also with the formation of AP

decomposition sites at microcrack intersections. SEM study of the initiation sites has been extended to nanometre dimensions with the atomic force microscope.

Acknowledgements

This work was supported by the US Office of Naval Research. We thank Drs E. Funk and Y. Q. Liu for help with the laser facilities, Dr W. L. Elban for supply of the T. L. Boggs-produced AP crystals, Drs W. T. Beard and K. A. Green for help with the X-ray orientation measurement, and Dr S. Javadpour for computer reconstruction of the stereographic projection diagram.

References

1. K. K. KUO, T. A. LITZINGER and W. H. HSIEH, in "Structure and Properties of Energetic Materials", Boston, November 1992, Vol. 246, edited by D. H. Liebenburg, R. W. Armstrong and J. J. Gilman (*Materials Research Society*, Pittsburgh, PA, 1993) p. 331.
2. A. L. RAMASWAMY, PhD thesis, Laser Ignition of Secondary Explosives, Cambridge University (1993).
3. R. W. ARMSTRONG, A. L. RAMASWAMY and J. E. FIELD, in "ONR/SNPE/ONERA Workshop on Combustion Mechanisms", ONREUR Report 91-02-w edited by R. W. Armstrong (US Office of Naval Research, European Office, London, 1991) 168.
4. F. SOLYMOSI, "Structure and Stability of Salts of Halogen Oxyacids in the Solid Phase" (Wiley, New York, 1977) p. 195.
5. H. W. SANDUSKY, B. C. GLANCY, D. W. CARLSON, W. L. ELBAN and R. W. ARMSTRONG, *J. Propulsion Power* **7** (1991) 518.
6. W. L. ELBAN, J. C. HOFFSOMMER and R. W. ARMSTRONG, *J. Mater. Sci.* **19** (1984) 552.
7. B. C. BEARD and J. SHARMA, in "Structure and Properties of Energetic Materials", Boston, November 1992, Vol. 246, edited by D. H. Liebenburg, R. W. Armstrong and J. J. Gilman (*Materials Research Society*, Pittsburgh, PA 1993) p. 257.
8. M. YOO, S. YOON and A. DE LOZANNE, *ibid.*, p. 221.
9. A. V. RAEVSKII and G. B. MANELIS, *Dokl. Akad. Nauk SSSR* **151** (1963) 886.
10. T. L. BOGGS and K. J. KRAEUTLE, *Comb. Sci. Technol.* **1** (1969) 75.
11. K. J. KRAEUTLE, *J. Phys. Chem.* **74** (1970) 1350.
12. K. J. KRAEUTLE, in "*Comb. Inst., Western States Section, Spring Meeting*", Pre-print 69–20 (1969).
13. J. SHARMA and C. S. COFFEY, A. L. RAMASWAMY and R. W. ARMSTRONG, in "Decomposition, Combustion and Detonation chemistry of Energetic Materials", Boston, November 1995, Vol. 418, edited by T. B. Brill, T. P. Russell, W. C. Tao and R. B. Wardle (*Materials Research Society*, Pittsburgh, PA, 1996) p. 257.
14. T. L. JOHNSTON, R. J. STOKES and C. H. LI, *Philos. Mag.* **7** (1962) 23.

Received 20 November 1995
and accepted 15 January 1996